Science Bulletin 64 (2019) 1110–1117

Contents lists available at ScienceDirect

Science Bulletin

journal homepage: www.elsevier.com/locate/scib

Article

Bio-inspired clamping microneedle arrays from flexible ferrofluid-configured moldings

Xiaoxuan Zhang [a,1], Fengyuan Wang [b,1], Yunru Yu [a,1], Guopu Chen [c], Luoran Shang [a,d], Lingyu Sun [a], Yuanjin Zhao [a,*]

[a] State Key Laboratory of Bioelectronics, School of Biological Science and Medical Engineering, Southeast University, Nanjing 210096, China
[b] Department of Dermatology, Zhongda Hospital, Southeast University, Nanjing 210009, China
[c] Department of General Surgery, Jinling Hospital, Medical School of Nanjing University, Nanjing 210002, China
[d] School of Engineering and Applied Sciences, Harvard University, Cambridge, MA 02138, USA

ARTICLE INFO

Article history:
Received 1 May 2019
Received in revised form 2 June 2019
Accepted 13 June 2019
Available online 20 June 2019

Keywords:
Bioinspired
Ferrofluids
Microneedle arrays
Drug release
Biomaterials

ABSTRACT

Microneedle (MN) arrays have demonstrated value for cosmetics, diagnosis, transdermal drug delivery, and other biomedical areas. Much effort has been devoted to developing simple stratagem for creating versatile moldings and generating functional MN arrays. Here, inspired by the serrated microstructure of mantises' forelegs, we present a novel serration-like clamping MN array based on ferrofluid-configured moldings. Benefiting from the flexibility and versatility of ferrofluids, negative microhole array moldings with various sizes and angles toward the midline could be created easily. The corresponding biocompatible polymer MN arrays with both isotropic and anisotropic structures could then be produced feasibly and cost-effectively by simply replicating these moldings. It was found that the resultant serrated clamping MN arrays had the ability to adhere to skin firmly, enabling them to be used over a relatively long time and while the recipient was moving. This proposed technology performed well in minimally invasive drug administration and sustained glucocorticoids release during treatment for imiquimod-induced psoriasis in mice. These features indicated that such MN arrays could play important roles in wearable transdermal drug delivery systems and in other applications.

1. Introduction

Microneedle (MN) arrays comprise a supporting pedestal and a series of orderly arranged micro-scale needles [1]. With typical lengths ranging from hundreds to thousands of microns and very sharp tips, the MN arrays can penetrate the skin, pass the stratum corneum, and form microchannels, without contacting intradermal nerve fibers and capillaries [2–5]. As a result, their transdermal delivery of various types of drugs could be enhanced dramatically, and skin trauma, pain and pathogenic infections could be reduced [6,7]. Such outstanding advantages make them an ideal choice in a variety of fields, including cosmetics [8], therapy [9,10] and so on. To develop the MN arrays, an effective stratagem is the use of different polymers [11–18] to replicate microhole array moldings [19–23], which are created by top-down approaches such as photolithography [24,25], computer-assisted laser ablation or etching [26–28], micro-printing [29], etc. [30–34]. With these negative moldings, a series of high-quality MN arrays have been achieved for different applications [35,36]. However, the creation of such moldings usually has some restrictions because of their high cost, low time efficiency, and technical demands. In addition, most of the top-down approaches could only create upright and symmetric MN arrays; the resultant arrays are prone to fall off the skin during motion and cannot resist many external forces, and these factors greatly limit their practical values as wearable drug delivery devices. Therefore, stratagems for creating versatile moldings and generating novel MN arrays are still anticipated.

In this paper, inspired by the serrated acicular structure of the forelegs of mantises, which imparts mantises with excellent grasping and holding properties, we present a novel serrated clamping MN array by using flexible ferrofluid-configured moldings (Fig. 1). Ferrofluids are uniform and stable colloidal liquid containing nanoscale ferromagnetic particles with diameters between 5 and 20 nm, which will disperse into small conical droplets and form actively tunable, dynamic, magnetically oriented patterns under a strong magnetic field [37–39]. By adjusting the orientation of the external magnetic field, the conical ferrofluid droplets could also rotate and tilt, so asymmetrical arrays could be generated to

* Corresponding author.
E-mail address: yjzhao@seu.edu.cn (Y. Zhao).
[1] These authors contributed equally to this work.

https://doi.org/10.1016/j.scib.2019.06.016
2095-9273/

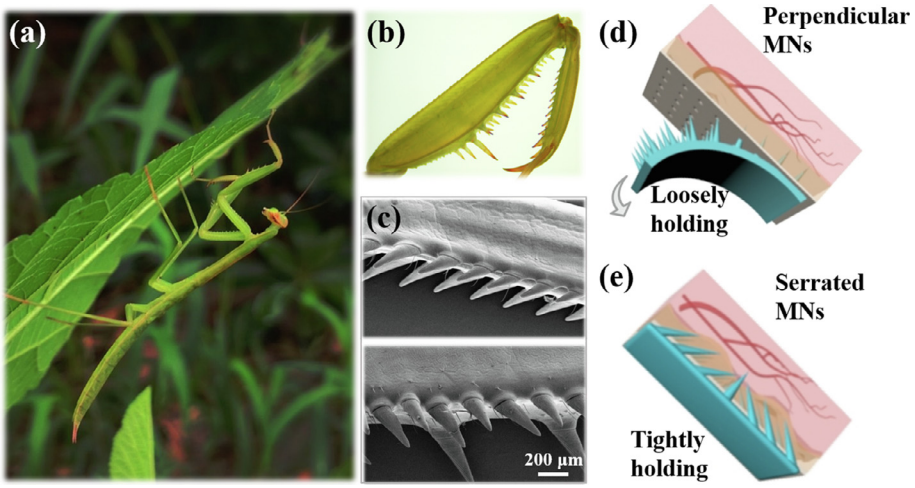

Fig. 1. (Color online) Schematic illustrations of bioinspired serrated clamping MNs. (a) Digital image of a mantis climbing on a leaf. (b, c) Optical and SEM images of the forelegs of mantises showing slant serrated microstructure. (d) Perpendicular MN array: the gray arrow shows it is prone to fall off from the skin when placed upside down. (e) Bio-inspired serrated clamping MN array has the ability to hold on firmly.

form marvelous moldings. Based on these ferrofluid-configured moldings, we could easily and cost-effectively produce biocompatible polymer replicas with different sizes and angles of serrated MNs leaning towards the midline. It was demonstrated that the replicated angled MN arrays were superior to perpendicular ones in many mechanical aspects, as they could remain firmly adherent when the attached substrate moved and rotated or even when subjected to external forces. Therefore, the prepared clamping MN arrays have great potential as ideal drug release devices, opening a new chapter in the biomedical application of MNs.

2. Experimental

2.1. Materials and animals

Organic-based ferrofluid (10% w/v) was obtained from Ferrotec Corp. (USA). Ethoxylated trimethylolpropane triacrylate (ETPTA, average $M_w \approx 912$), 2-hydroxy-2-methylpropiophenone (HMPP), Sorbitan monooleate (Span 80), Poly(ethylene glycol) diacrylate (PEGDA, average $M_w \approx 700$) and Rhodamine B (≧95%, HPLC) were purchased from Sigma-Aldrich Corp. Lyophilized silk fibroin was derived from Simatech Corp. (China). Imiquimod was bought from Sichuan Med-shine Pharmaceutical Corp. Budesonide was provided by Astrazeneca Corp. The PBS buffer and porcine cadaver skin were prepared in the laboratory. Deionized water with a resistivity of 18.2 MΩ cm^{-1} was purified through a Millipore Milli-Q system. All chemical reagents were of the best grade available and used as received. The 10–12 weeks male BALBc mice were supplied by Jinling Hospital. Animals were treated in strict accordance with the recommendations in the Guide for the Care and Use of Laboratory Animals of the National Institutes of Health, USA. All the animal care and experimental protocols were reviewed and approved by Animal Investigation Ethics Committee of Jinling Hospital.

2.2. Fabrication of the negative mold

2 mL of UV-curable agent ETPTA (average $M_w \approx 912$) pre-mixed with photoinitiator HMPP (1% v/v) and additive Span 80 (10% v/v) were added into a petri dish using pipettor. Then 5 μL of organic-based ferrofluid was dispersed and submerged by the prepolymer mixture. A large, cylindrical permanent magnet (4000 GS, with 6 cm in diameter and 1 cm in height) was placed under the petri dish to provide a relatively homogeneous magnetic field. By adjusting the distance between the magnet and the petri dish, the ferrofluid broke up into conical droplets and formed arrays with desired size. The magnet was then rotated clockwise to provide tilted magnetic field, and a shutter was placed above the middle and right part of prepolymer mixture to block light. The left part was solidified under the UV-light (EXFO OmniCure SERIES 1000, 365 nm, 100 W) for 25 s. The magnet was then rotated anticlockwise, the middle part was shaded and the right part was cured by UV radiation. Finally, the magnet was placed horizontally and the middle part was UV solidified. The solidified ETPTA negative mold was immersed in PBS buffer solution and gently stripped out of the petri dish. Then it was washed by ethanol and deionized water for 3 times by means of ultrasonic cleaning, respectively. The negative mold was thus obtained and stored in deionized water to avoid occurrence of cracks.

2.3. Fabrication of the serrated clamping MN array

50 μL of silk fibroin solution (30% w/v) was applied to the negative mold and kept in vacuum pump for 20 min to fully fill the cavities. Then the redundant silk fibroin solution was sucked up using pipettor. The silk fibroin was dried for 2 h at room temperature to form the outer layer of the tips. 300 μL of PEGDA (average $M_w \approx 700$) mixed with photoinitiator HMPP (1% v/v) was then added to negative mold and kept in vacuum pump for 20 min to fill the gaps. The mixture was then cured by UV irradiation for 30 s under the UV-light system (EXFO OmniCure SERIES 1000, 365 nm, 100 W) to form the inner layer. Eventually the resultant MN arrays were peeled out of the negative mold by dipping in PBS buffer solution.

2.4. Characterization

The dynamic response of ferrofluid droplets, the negative molds with different inclination angles and sizes as well as the MN arrays replicated from negative molds were observed under a stereomicroscope (Olympus BX51) and captured by CCD (AOS Technologies AG). Color photos and videos were taken by a digital camera (Canon 5D Mark II). SEM images were obtained using a scanning electron microscope (SEM, Hitachi S-3000N). The fluorescence intensity of RhB was detected by a multimode plate reader

(Synergy HTX, BioTek). The fluorescence image was acquired by a microscopy (Olympus IX71) and CCD (Olympus DP30BW).

2.5. Rotation, holding time and load bearing test

Newly bought porcine cadaver skin was adhered to a clean glass slide. The MN arrays were incurved to make the tips face toward the porcine skin. After piercing the skin, the MN arrays returned back to their former flat state and remained pressed with a constant force for 30 s. The MN-attached porcine skin was then rotated from 0° to 180° and whether the arrays would fall from the skin during rotation process was observed. Then the MN-applied porcine skin was placed vertically, 135-degree slantly and inversely and the falling time of the arrays was recorded. Based on the holding time test, small cylindrical magnets (5 mm in diameter, 1.5 mm in thickness and about 0.2 g in weight; 5 mm in diameter, 1 mm in thickness and about 0.12 g in weight) were attached to the applied MN arrays one by one until the arrays fell off from the porcine cadaver skin. The cylindrical magnets were weighed by an electronic scales (Techcomp, FA1204B) and the maximum bearing weight was calculated.

2.6. In vivo adhesion ability test

The mice were anesthetized by intraperitoneal injection of 10% (w/v) chloral hydrate and the flank side was shaved with an electric clipper and treated with depilatory cream. The exposed flank skin was then washed with ethanol (75% v/v) and dried in the air. The serrated MN arrays were adhered to the skin in the same way. The mice were then placed in a transparent box as well as an exercise wheel and observed for 20 min, respectively.

2.7. In vitro drug sustained release

Redundant PEGDA pedestals were first cut off from the MN array patches and the inner PEGDA layer of the tips was preserved, as the tips played the major role in drug delivery in vivo. The patches were immersed in RhB solution (1 mg mL^{-1}) for 2 days. The RhB-loaded patches were then picked up and washed by PBS buffer solution (pH 7.4) to clear away surface RhB solution. Subsequently, the patches were placed in a 24-well plate (Thermo, USA), submerged in PBS and shook on a thermomixer (Eppendorf, 28 °C, 450 r min^{-1}). The concentration of RhB was monitored by a multimode plate reader (540 nm excitation wavelength) and calculated from the standard curve of RhB. The loading efficiency and cumulative release were defined as the following functions:

$$\text{Loading efficiency}(\%) = \frac{\text{Loading amount of RhB(g)}}{\text{Weight of microneedle array(g)}} \times 100\%,$$

$$\text{Cumulative release}(\%) = \frac{\text{Real time amount of RhB(mg)}}{\text{Loading amount of RhB(mg)}} \times 100\%.$$

The loading amount of RhB was measured by calculating the concentration variation of the prepared RhB solution based on the following function:

$$\text{Loading amount of RhB} = V_{\text{before}} \times C_{\text{before}} - V_{\text{after}} \times C_{\text{after}} - V_{\text{wash}} \times C_{\text{wash}},$$

where V_{before}, V_{after} and V_{wash} were the volume of the prepared RhB solution before immersing MNs, RhB solution after immersing MNs and the PBS solution used to wash MNs, respectively; while C_{before}, C_{after} and C_{wash} were the RhB concentration of the prepared RhB solution before immersing MNs, RhB solution after immersing MNs and the PBS solution used to wash MNs, separately.

2.8. Dermal toxicity and skin penetration test (in vivo)

The mice were anesthetized by intraperitoneal injection of 10% chloral hydrate. Hair on the back of the skin was removed using an electric clipper as well as depilatory cream. The serrated MN arrays were then inserted into the dorsal skin by hand in the same way as mentioned and remained tightly pressed for 2 min. The dorsal skin was observed by a stereomicroscope (Olympus BX51) until the insertion marks disappeared completely.

2.9. In vivo drug delivery

The 10–12 weeks male BALBc mice were shaved with an electric clipper and treated with depilatory cream to remove back hair. 70 mg of imiquimod was applied to the hair-free backs once a day for seven consecutive days to establish the psoriasis model. Then the mice were divided into four groups for therapeutic experiments. Three groups were treated with empty silk fibroin-PEGDA MN array patches, budesonide suspension (0.5 mg mL^{-1}) and budesonide loaded MN patches, respectively. The budesonide loaded MN patches were prepared using budesonide (0.5 mg mL^{-1})/silk fibroin solution and budesonide (0.5 mg mL^{-1})/PEGDA as materials by the aforementioned molding method. The other group was used as blank control. The mice were sacrificed after 3 days and the tissue around the skin lesions was removed, fixed in 4% paraformaldehyde and embedded in paraffin. Sections were stained with hematoxylin-eosin for further histopathological examination.

3. Results and discussion

In a typical experiment, the mantis-foreleg-inspired microstructures were replicated from dynamic ferrofluid-configured moldings. Mantises could hold objects tightly with their forelegs (Fig. 1a), inspiring us to observe their microstructure and to mimic them to enhance adhesion. For this purpose, the anatomical features of forelegs were characterized using scanning electron microscopy (SEM) and optical microscopy. It was found that rows of tiny serrated sharp spikes line up in an orderly fashion on the surface of the forelegs, ranging from 200 to 900 μm in length and from 40° to 80° in inclination angle, as shown in Fig. 1b, c. As there are no other special features in the spikes, the serrated slant shape of the spikes should play a pivotal role in the adhesive ability of the mantis forelegs. In addition, considering that the first two sections of the mantises' forelegs would fold and form a clamping structure when holding objects, we designed MNs with similar serrated clamping structure whose tips slanting toward the central row to improve the adhesion ability. However, it is difficult to achieve such a feature by conventional top-down approaches, such as photolithography and laser ablation. Therefore, considering their flexibility and tunability, ferrofluid droplets were chosen to form moldings of slant serrated arrays and to serve as the master structures for MN fabrication (Fig. 2a).

Because of magnetic hydrodynamic instability, ferrofluids could be broken into separate conical droplets in the non-magnetizable ultraviolet (UV) curing prepolymer mixture when a large cylindrical magnet was placed below. It was found that by rotating the external magnet from its original longitudinal axis orientation toward the transverse plane, the ferrofluid droplets followed the correspondingly tilted magnetic induction lines and slanted accordingly. When the magnet rotation angle increased, the angle between the droplets and the horizontal plane decreased (Fig. 2b–d and Fig. S1a online). Notably, besides the inclination angle, the size of the master structure could also be tailored. By moving the external magnet longitudinally downward, the MNs

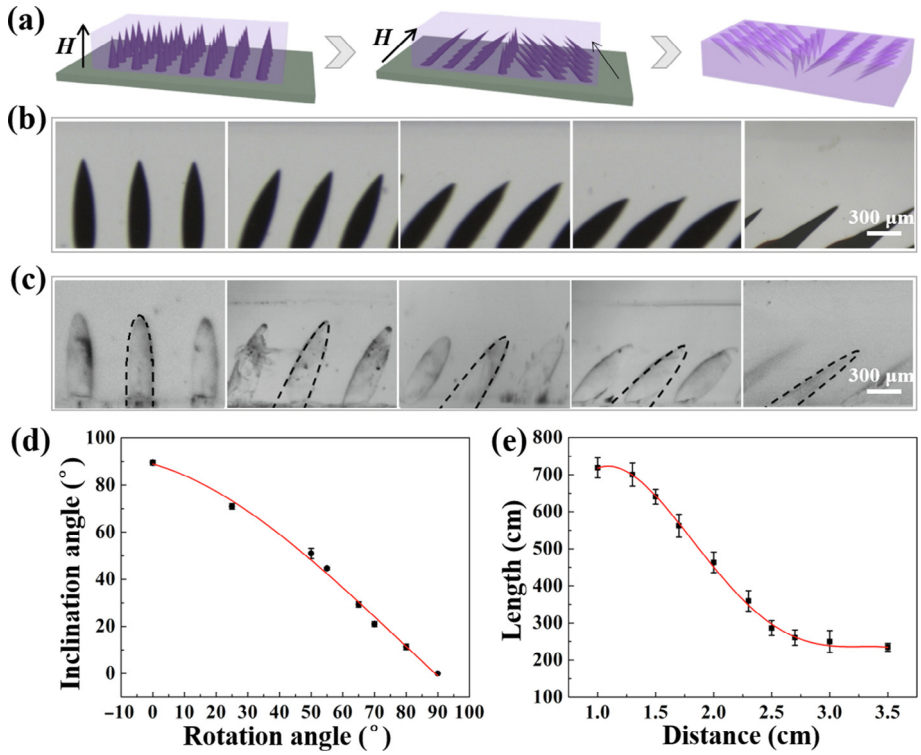

Fig. 2. (Color online) Negative molds fabricated from highly adjustable ferrofluid moldings. (a) Schematic illustration of negative mold fabricated by molding of orderly arranged ferrofluid droplets under magnetic field. "*H*" represents the magnetic field direction. (b) Optical microscope images of the dynamic assembly behavior of ferrofluid droplets in response to rotated external magnetic field. (c) Optical microscope images of ETPTA molds from ferrofluid master mold with different inclination angles. (d) Relationship between inclination angle of MN and rotation angle of magnet. (e) Relationship between length of MN and the distance between magnet and substrate.

shortened because the reduced magnetic strength allowed the constraint interfacial tension to predominate over the magnetic lifting force (Fig. S1b online). In addition, by increasing the distance between the magnet and substrate, the droplets contracted vertically, and the edges and tips became smoother and flatter (Fig. 2e and Fig. S2 online). It should also be mentioned that the maximal length of the ferrofluid droplet is limited by the concentration of ferromagnetic particles in ferrofluids. Because of this, the growth rate of the droplet length greatly slowed down when the distance was shorter than 1 cm.

Benefiting from the instantaneity of UV curing of the prepolymer mixture, the negative molds that perfectly duplicated the flexible ferrofluid configured moldings could be fabricated successfully. As diverse arrays of the ferrofluid droplets could be formed by adjusting the magnetic field parameters, a range of negative molds with cavities of different inclination angles and depths could be replicated. It is worth mentioning that by step-curing the prepolymer, negative molds with anisotropic angled microholes could also be produced. During this process, the magnet was first rotated clockwise to provide a tilted magnetic field with a shutter placed above the middle and right part to block light, and only the left part was solidified by UV radiation. Using the same means, the right and middle parts were then cured under left-slanting and straight magnetic fields successively, as shown in Fig. S3 (online). The ferrofluid could then be washed off and clean negative molds could be created with grooves inclining from both sides to the center.

Based on the resultant negative mold, silk fibroin hydrogel MN arrays with angled clamping structures could be fabricated. Although the silk fibroin hydrogels were well biocompatible and performed well in drug release, their formed MNs were prone to collapse after drying. To solve this problem, poly-(ethylene glycol) diacrylate (PEGDA) was also added to increase the rigidity of the silk fibroin MNs. In this process, the silk fibroin solution was first cast as the outer layer of the tips. Then the PEGDA solution was infiltrated to form the inner layer of the tips and the pedestal. Finally, serrated clamping MN arrays with the desirable stiffness properties could be fabricated by detaching them from the negative molds (Fig. 3a). The generated MN arrays with inclination angles ranging from 30° to 90° well replicated the structure of the negative mold and achieved approximation to the sizes and inclination angles of the serrated spikes on mantises' forelegs, indicating a successful fabrication strategy (Fig. 3b–f and Figs. S4, S5 online). It should also be mentioned that as both silk fibroin and PEGDA were stable biomaterials, these MN arrays possess wonderful stability, which could be stored in proper conditions for months and remain intact for days in a physiological state.

Notably, different from the ordinary perpendicular MN arrays, the serrated clamping MNs showed improved adhesion properties. To demonstrate this, MN array patches with different inclination angles were applied to the skin of porcine cadavers. To ensure that they were attached successfully, the patches were first incurved to make the tips face toward the skin surface. After piercing the skin, the patches recovered to their previous flat state and remained pressed for a constant time, as shown in Fig. S6 (online). Then the skin together with the applied patch was rotated from 0° to 180°, and the holding times as well as maximum bearing weights were recorded accordingly (Fig. 4a, b and Fig. S7 online). It was observed that during this rotation process, all MN arrays could hold onto the skin firmly. With increased MN angles plus decreased rotation angles, the holding time and the bearing weight were all increased (Fig. 4c, d). In particular, at the vertical position, the holding times of all serrated clamping MN arrays were more than 30 min. This improved adhesive ability could be attributed to the increased grasping force caused by the centrally oriented structures of the serrated clamping MN arrays.

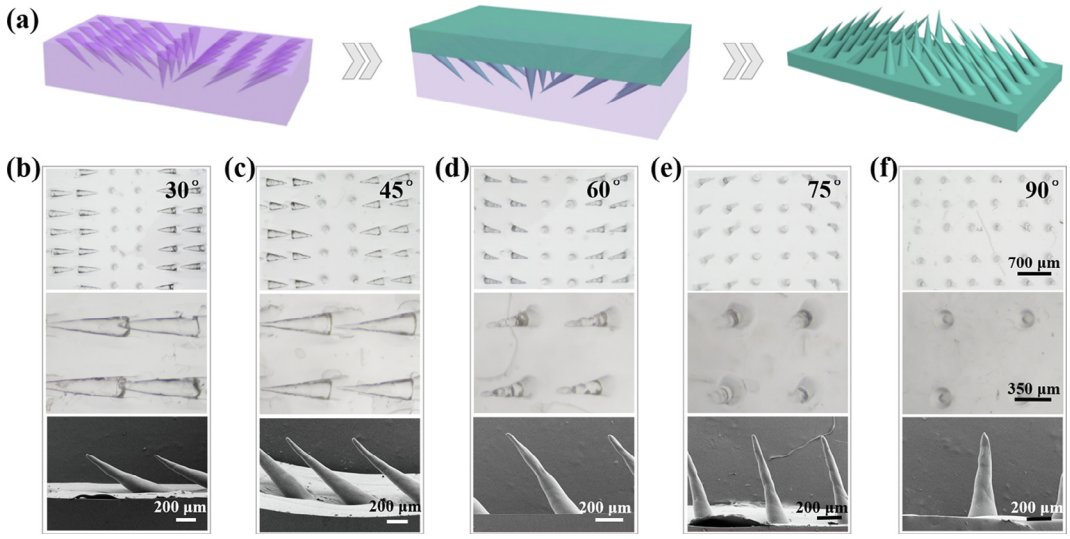

Fig. 3. (Color online) Fabrication and characterization of serrated clamping MN arrays. (a) Schematic illustration of the fabrication process. (b–f) Optical and SEM images of MNs with different inclination angles of 30° (b), 45° (c), 60° (d), 75° (e), 90° (f).

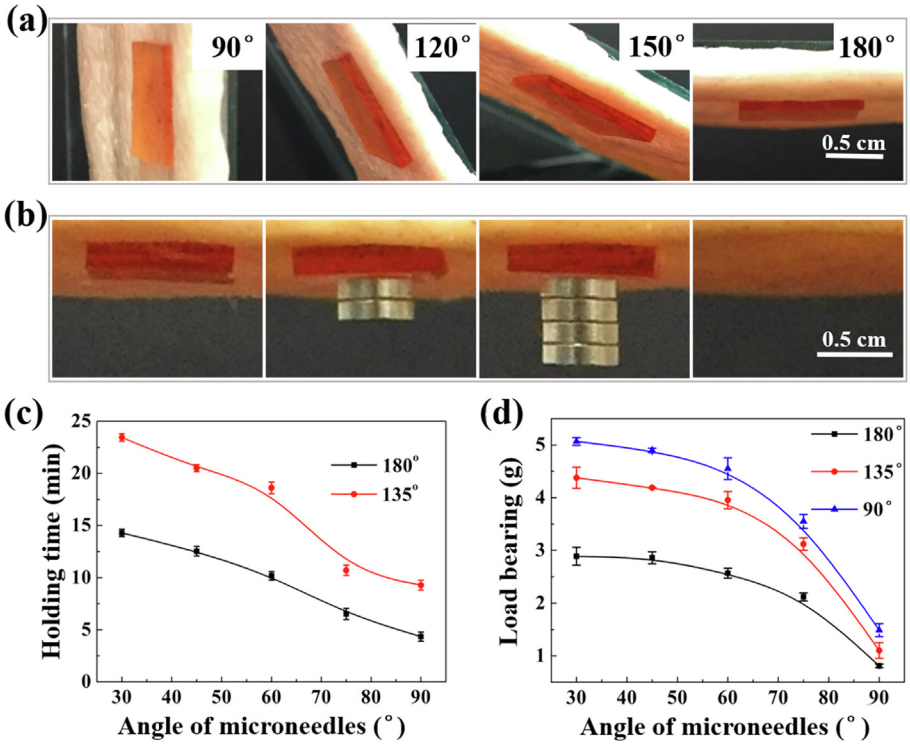

Fig. 4. (Color online) Adhesion property tests of the serrated clamping MN arrays. (a) Digital images of the MN array holding onto the skin during rotation. (b) Digital images of external weight addition process. (c) Maximum holding time as function of MN inclination angles when the patch-applied skin was placed in 135° and 180°. (d) Maximum load bearing as function of MN inclination angle when the patch-applied skin was placed in 90°, 135° and 180°.

To mimic the practical application situations of this adhesive ability better, the serrated clamping MN arrays were also applied to the flanks of mice, as recorded in Movie S1 (online). It was found that compared with the perpendicular MN array, which fell off the mice skin very quickly, the serrated clamping MN arrays remained well attached to the skin even if the mice were moving constantly. As the limited penetration depth caused by the excess tilt of the MNs had greater influence on the adhesion performance on the skin of live mice, the inclination angle of the serrated clamping MN arrays should be no more than 30° to enable the easy insertion. These results confirmed that with excellent firmness and stability, these serrated clamping MN arrays could have enormous potential for practical use.

Besides the improved adhesion ability, the prepared MN arrays could also be good candidates for sustained drug delivery. The release kinetics of Rhodamine B (RhB), a model for low-molecular-weight hydrophilic drugs, from the silk fibroin-PEGDA MN arrays with different inclination angles, silk fibroin concentrations and heights were recorded, respectively. The results showed that the inclination angles had little influence on loading efficiency

(Fig. 5a), and RhB release showed an initial rapid rise, followed by a long-term release and then a sustained equilibrium that was not influenced by the inclination angles either (Fig. 5b). In addition, the increased loading efficiency and the decreased RhB release rate suggested the increased overall drug dosage and prolonged drug action time, which could be attributed to the outstanding drug

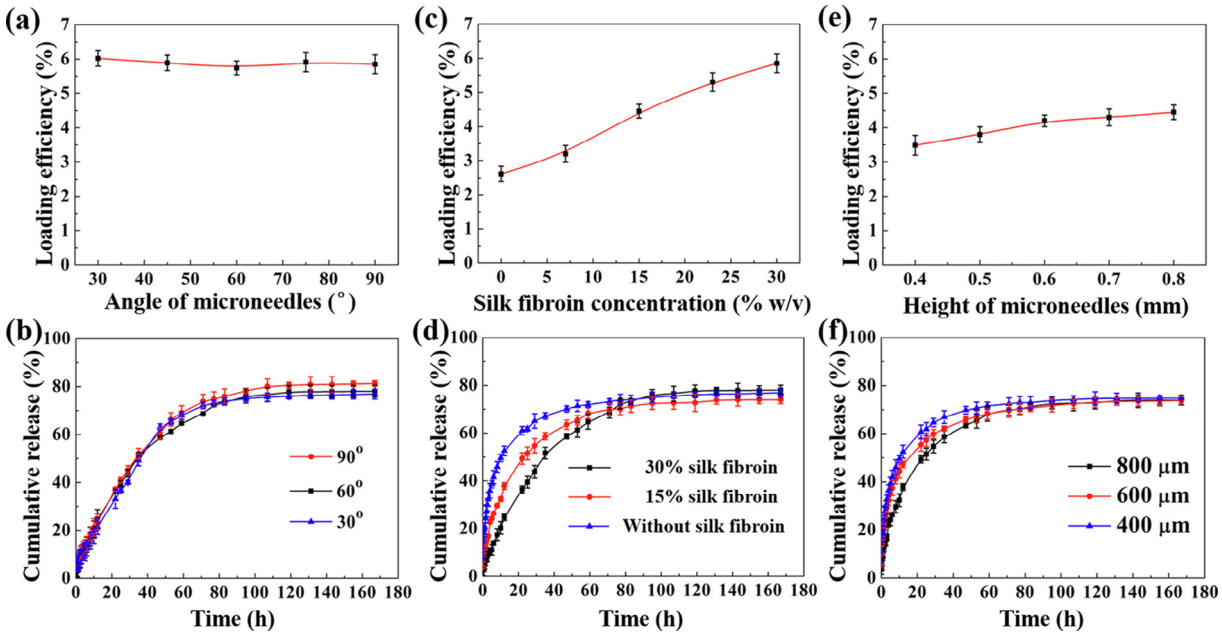

Fig. 5. (Color online) In vitro RhB release from MNs. (a, b) The relationships between RhB loading efficiency plus cumulative RhB release and the MN inclination angle. (c, d) The relationships between RhB loading efficiency plus cumulative RhB release and the silk fibroin concentration. (e, f) The relationships between RhB loading efficiency plus cumulative RhB release and the MN height.

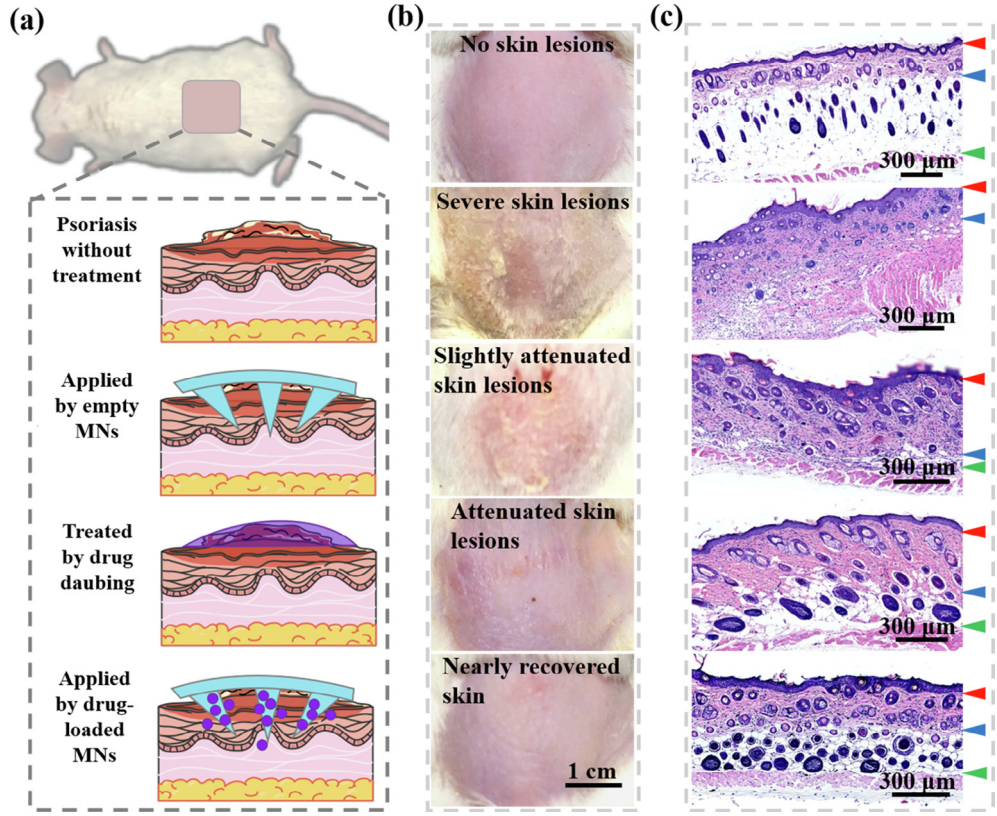

Fig. 6. (Color online) Treatment for imiquimod-induced psoriasis in mice. (a) Scheme of normal mouse dorsal skin and different treatments for the four groups of imiquimod-induced psoriasis mice. (b) Digital images of the corresponding dorsal skin after 3 days of therapy. (c) Hematoxylin-eosin staining of dorsal skin after 3 days of therapy (above the red triangle: epidermis; above the blue triangle: dermis; above the green triangle: fat; below the green triangle: muscle).

release properties of the added silk fibroin (Fig. 5c and d). It was also found that the loading efficiency increased slightly while the release rate decreased a little when the MNs had been elongated, probably because the increase of the length led to the increase of relative content of silk fibroin in tips, as shown in Fig. 5e, f.

Before moving to practical applications, the serrated clamping MN arrays were applied to mouse skin to test their puncturing ability and security. They were first inserted into the shaven dorsal skin as described above. After the MNs had been removed carefully, the skin surface exhibited an obvious array of microholes corresponding to the sites where MNs had been inserted, indicating successful insertion. As the skin slowly recovered, the penetration marks gradually became invisible. Finally, the marks vanished almost completely, and there were no serious adverse reactions such as apparent injury, signs of inflammation, or other abnormal clinical changes, as shown in Fig. S8 (online). The rapid recovery of skin confirmed that the administration of MNs was safe and minimally invasive. In addition, to demonstrate that the serrated clamping MN arrays have ability to deliver drug into skin efficiently, MNs loaded with fluorochrome were also applied to mouse skin. It was found from the fluorescence image that the fluorochrome could diffuse from the MNs to the microholes generated by MNs and be absorbed by skin, indicating an efficient drug delivery (Fig. S9 online).

To explore the practical value of our MN arrays, we encapsulated glucocorticoids within them, established a mouse model of imiquimod-induced psoriasis and examined their in vivo efficacy in treating this disease. The mice were divided into four groups: untreated controls, those receiving empty MN arrays, those receiving direct glucocorticoid daubing to the skin, and those treated with glucocorticoid-loaded MN arrays (glu-MNs) (Fig. 6a). Because glucocorticoid could attenuate psoriasiform skin inflammation symptoms such as erythema, skin scaling, and parakeratosis, both the glucocorticoid-daubed and glu-MNs-treated groups showed obvious recovery of skin lesions (Fig. 6b, c). Notably, the therapeutic effects appeared to be superior at the same dose regimen in glu-MNs-treated group, proved by less skin thickening, reduced acanthosis, suppressed leukocyte infiltration and clearer skin layers shown in gross presentation and corresponding histology (Fig. S10 online). The results confirmed the enhanced drug delivery and absorption provided by these arrays. It should also be mentioned that the empty-MNs-applied group also showed improved skin conditions, probably because physical stimulation from the MN insertion enhanced skin metabolism. Thus, thanks to the versatility of MN-assisted drug delivery, the serrated clamping MN arrays could be used for administering a wide range of drugs for disease treatment, indicating that they might open a new chapter for wearable transdermal drug delivery devices.

4. Conclusion

In summary, we have fabricated novel biomimicking serrated clamping MN arrays with a microstructure similar to the forelegs of mantises, based on flexible ferrofluid-configured moldings. These ferrofluid derived moldings could be formed with controllable inclination angles as well as sizes, and they could serve as dynamic master structures by adjusting the magnetic orientation and field strength. Then, using a stepwise UV curing method, the serrated clamping MN arrays with desired features could be replicated easily, effectively, controllably, and continuously. This method is repeatable to be scaled up and suitable for further commercial manufacture, as the negative molds could be used for many times to generate MNs. The serrated clamping structures enabled the resultant MN arrays to pierce skin and to hold on to skin firmly, even when submitted to external loading or movements. Although the MN arrays showed excellent adhesion ability, the removal of them would not cause much pain as they were made from soft materials and did not contact with intradermal nerve fibers. Additionally, the fabricated MN arrays could perform well in sustained drug release in vitro and skin penetration in vivo. By loading glucocorticoids, these serrated clamping MN arrays could also greatly enhance drug delivery and absorption, thereby improving treatment for imiquimod-induced psoriasis in mice. These features make them highly favorable to serve as wearable drug delivery devices, broadening its functionality and application fields to a high degree.

Conflict of interest

The authors declare that they have no conflict of interest.

Acknowledgments

This work was supported by the National Key Research and Development Program of China (2017YFA0700404), the NSAF Foundation of China (U1530260), the Natural Science Foundation of Jiangsu (BE2018707), the Scientific Research Foundation of Southeast University, and the Scientific Research Foundation of the Graduate School of Southeast University.

Author contributions

Y. J. Z. conceived the idea and designed the experiment. X. X. Z. and F. Y. W. carried out the experiments. X. X. Z. and Y. R. Y. analyzed data and wrote the paper. G. P. C. assisted with experiment operations. L. Y. S. and L. R. S. contributed to scientific discussion of the article. X. X. Z., F. Y. W. and Y. Y. R. contributed equally to this work.

Appendix A. Supplementary data

Supplementary data to this article can be found online at https://doi.org/10.1016/j.scib.2019.06.016.

References

[1] Ye YQ, Wang C, Zhang XD, et al. A melanin-mediated cancer immunotherapy patch. Sci Immunol 2017;2:eaan5692.
[2] Zhang YQ, Yu JC, Wang JQ, et al. Thrombin-responsive transcutaneous patch for auto-anticoagulant regulation. Adv Mater 2017;29:1604043.
[3] Ma GJ, Wu CW. Microneedle, bio-microneedle and bio-inspired microneedle: a review. J Control Release 2017;251:11–23.
[4] Ye YQ, Yu JC, Wen D, et al. Polymeric microneedles for transdermal protein delivery. Adv Drug Deliver Rev 2018;127:106–18.
[5] Wang JQ, Ye YQ, Yu JC, et al. Core-shell microneedle gel for self-regulated insulin delivery. ACS Nano 2018;12:2466–73.
[6] Lee H, Song C, Baik S, et al. Device-assisted transdermal drug delivery. Adv Drug Deliver Rev 2018;127:35–45.
[7] Zhang YQ, Liu QM, Yu JC, et al. Locally induced adipose tissue browning by microneedle patch for obesity treatment. ACS Nano 2017;11:9223–30.
[8] Larraneta E, Lutton REM, Woolfson AD, et al. Microneedle arrays as transdermal and intradermal drug delivery systems: materials science, manufacture and commercial development. Mat Sci Eng R 2016;104:1–32.
[9] Yu JC, Qian CG, Zhang YQ, et al. Hypoxia and H_2O_2 dual-sensitive vesicles for enhanced glucose-responsive insulin delivery. Nano Lett 2017;17:733–9.
[10] Hu XL, Yu JC, Qian CG, et al. H_2O_2-responsive vesicles integrated with transcutaneous patches for glucose-mediated insulin delivery. ACS Nano 2017;11:613–20.
[11] Fu FF, Chen ZY, Zhao Z, et al. Bio-inspired self-healing structural color hydrogel. Proc Natl Acad Sci USA 2017;114:5900–5.
[12] Wang J, Zou MH, Sun LY, et al. Microfluidic generation of buddha beads-like microcarriers for cell culture. Sci China Mater 2017;60:857–65.
[13] Zhang YS, Khademhosseini A. Advanced in engineering hydrogels. Science 2017;356:eaaf362.
[14] Song Y, Michaels TCT, Ma QM, et al. Budding-like division of all-aqueous emulsion droplets modulated by networks of protein nanofibrils. Nat Commun 2018;9:2110.

[15] Meng JX, Zhang PC, Wang ST. Recent progress of abrasion-resistant materials: learning from nature. Chem Soc Rev 2016;45:237–51.
[16] Zhang XW, Wang J, Jin H, et al. Bioinspired supramolecular lubricating hydrogel induced by shear force. J Am Chem Soc 2018;140:3186–9.
[17] Balasubramanian V, Herranz-Blanco B, Almeida PV, et al. Progress in polymer science. Prog Polym Sci 2016;60:51–85.
[18] Zhang Q, Li YC, Lin ZY, et al. Electrospun polymeric micro/nanofibrous scaffolds for long-term drug release and their biomedical applications. Drug Discov Today 2017;22:1351–66.
[19] Fu FF, Shang LR, Chen ZY, et al. Bioinspired living structural color hydrogels. Sci Robot 2018;3:eaar8580.
[20] Liu MJ, Wang ST, Jiang L. Nature-inspired superwettability systems. Nat Rev Mater 2017;2:17036.
[21] Bhatnagar S, Dave K, Venuganti VVK. Microneedles in the clinic. J Control Release 2017;260:164–82.
[22] Song Y, Shimanovich U, Michaels TCT, et al. Fabrication of fibrillosomes from droplets stabilized by protein nanofibrils at all-aqueous interfaces. Nat Commun 2016;7:12934.
[23] Sun JS, Zhang L, Wang JL, et al. Tunable rigidity of (polymeric core)-(lipid shell) nanoparticles for regulated cellular uptake. Adv Mater 2015;27:1402.
[24] Shang LR, Cheng Y, Zhao YJ. Emerging droplet microfluidics. Chem Rev 2017;117:7964–8040.
[25] Wang H, Zhao Z, Liu YX, et al. Biomimetic enzymes cascade reaction system in microfluidic electrospray microcapsules. Sci Adv 2018;4:eaat2816.
[26] Liu DF, Zhang HB, Fontana F, et al. Current developments and applications of microfluidic technology toward clinical translation of nanomedicines. Adv Drug Deliver Rev 2018;128:54–83.
[27] Li W, Liu ZH, Fontana F, et al. Tailoring porous silicon for biomedical applications: from drug delivery to cancer immunotherapy. Adv Mater 2018;30:1703740.
[28] Martins JP, D'Auria R, Liu DF, et al. Engineered multifunctional albumin-decorated porous silicon nanoparticles for fcrn translocation of insulin. Small 2018;14:1800462.
[29] Jia WT, Gungor-Ozkerim PS, Zhang YS, et al. Direct 3D bioprinting of perfusable vascular constructs using a blend bioink. Biomaterials 2016;106:58–68.
[30] Zhang Z, Kong XY, Xiao K, et al. A bioinspired multifunctional heterogeneous membrane with ultrahigh ionic rectification and highly efficient selective ionic gating. Adv Mater 2016;28:144.
[31] Liu DF, Zhang HB, Cito S, et al. Core/shell nanocomposites produced by superfast sequential microfluidic nanoprecipitation. Nano Lett 2017;17:606–14.
[32] Xu TL, Gao W, Xu LP, et al. Fuel-free synthetic micro/nanomachines. Adv Mater 2017;29:1603250.
[33] Sun XM, Lang Q, Zhan HB, et al. Electrospun photocrosslinkable hydrogel fibrous scaffolds for rapid in vivo vascularized skin flap regeneration. Adv Funct Mater 2017;27:1604617.
[34] Li XY, Jiang XY. Microfluidics for producing poly(lactic-*co*-glycolic acid)-based check for pharmaceutical nanoparticles. Adv Drug Deliver Rev 2018;128:101–14.
[35] Chen ZW, Hu QY, Gu Z. Leveraging engineering of cells for drug delivery. Acc Chem Res 2018;51:668–977.
[36] Amjadi M, Sheykhansari S, Nelson BJ, et al. Recent advances in wearable transdermal delivery systems. Adv Mater 2018;30:1704530.
[37] Shang LR, Yu YR, Gao W, et al. Bio-inspired anisotropic wettability surfaces from dynamic ferrofluid assembled templates. Adv Funct Mater 2018;28:1705802.
[38] Tsai SSH, Wexler JS, Wan JD, et al. Conformal coating of particles in microchannels by magnetic forcing. Appl Phys Lett 2011;99:153509.
[39] Chen HS, Zhao YJ, Li J, et al. Reactions in double emulsions by flow-controlled coalescence of encapsulated drops. Lab Chip 2011;11:2312–5.

Xiaoxuan Zhang received her bachelor's degree from the School of Biological Science and Medical Engineering of Southeast University in 2019. She is now a Ph.D. student under the supervision of Prof. Yuanjin Zhao at the State Key Laboratory of Bioelectronics of Southeast University. Her current scientific interests focus on microneedles and their applications.

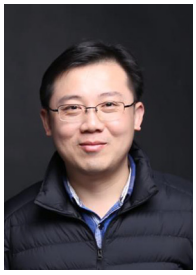

Yuanjin Zhao is a full professor at the School of Biological Science and Medical Engineering of Southeast University. He received his Ph.D. degree in 2011 from the School of Biological Science and Medical Engineering of Southeast University. In 2009–2010, he worked as a research scholar in Prof. David A. Weitz's group in Harvard University. His current scientific interests include microfluidics, ferrofluids, biomaterials, and organs-on-chips.